Macromolecules
ARTICLE

Macromolecules **2009**, *42*, 4181–4190 **4181**
DOI: 10.1021/ma900090j

Molecular Dynamics of PEGylated Multifunctional Polyhedral Oligomeric Silsesquioxane

Yu Bian and Jovan Mijović*

Othmer-Jacobs Department of Chemical and Biological Engineering Polytechnic Institute of New York University Six Metrotech Center, Brooklyn, New York 11201

Received January 15, 2009; Revised Manuscript Received April 24, 2009

ABSTRACT: Here we report a study of molecular dynamics of (1) four different poly(propylene oxide)/poly (ethylene oxide) (PPO/PEO) copolymers, two amorphous and two semicrystalline, and (2) the product of the chemical reaction between these copolymers and a multifunctional polyhedral oligomeric silsesquioxane (POSS). We refer to the latter group of compounds as "PEGylated POSS". Experimental results were generated using broadband dielectric relaxation spectroscopy (DRS) and dynamic mechanical spectroscopy (DMS) over a wide range of frequencies and temperatures. Amorphous copolymers exhibit the segmental process (α), the normal mode process (α_N), and two local processes (β and γ), while semicrystalline copolymers possess segmental (α) and two local relaxations (β and γ). The β process is a secondary relaxation and the γ process is due to the combination of the local motions in PPO and PEO blocks. PEGylated POSS was synthesized by chemical reaction between the functional end groups on the PPO block (amine) and the POSS side chain (epoxy). Dynamics of PEGylated POSS were investigated and contrasted with the dynamics of the corresponding neat copolymers. Covalent bonding between POSS and copolymer slows down the segmental and the normal mode process but does not affect the time scale of the β or the γ process. A detailed account of the effect of molecular weight, PPO/PEO mole ratio, copolymer morphology and covalent bonding between POSS and copolymer on the molecular origin, temperature dependence, and spectral characteristics of relaxation processes in copolymers and PEGylated POSS is provided.

Introduction

Nanoparticles play an important role in a wide variety of applications that include fuel cells,[1] catalysts,[2] coatings,[3,4] and lubricants.[5] One particularly promising sector where nanoparticles are projected to have a major impact is biomedicine.[6−8] Nanoparticles can be used to deliver drugs and genes,[9] detect proteins,[10] probe the DNA structure,[11] and make tissue scaffolds.[12] Most nanoparticles used in biological and medicinal fields are organic materials, such as liposomes[13−15] or polymeric nanoparticles;[16−19] they are biocompatible, nontoxic, and biodegradable. There is, however, a considerable current research interest in inorganic nanoparticles due to their low weight and excellent mechanical, electrical and thermal properties.[20−23] For instance, carbon nanotubes (CNT) are used as biomedical sensors.[24] Exciting work on CNT sensors has been recently reported by the Strano group.[25−29] A sensor made of CNT with attached DNA can be used to trace the cancer-causing toxin in living cells by following the change in the fluorescent light signal as a function of the sensor/DNA interactions inside the cell.

Most recently, there have been reports of the use of inorganic−organic nanoparticles for biomedical applications. Examples of such nanoparticles, which combine the advantages of organic and inorganic materials, include a range of inorganic−organic hybrid core/shell nanostructures.[30−32] Among inorganic−organic nanoparticles, the family of oligomeric polyhedral silsesquioxanes (POSS) has received particular attention. POSS compounds embody a truly hybrid architecture of an inner inorganic framework made up of silicone and oxygen $(SiO_{1.5})_x$ externally covered by organic substituents.[33−36] POSS can be easily chemically functionalized and its derivatives can withstand a variety of harsh thermal and chemical conditions.[37−40] The interest in the use of silica-based materials in biomedicine stems from their chemical inertness and biocompatibility,[41,42] however, there is a paucity of data on POSS for the use in this field. In fact there is only one reported study that has explored a possible use of POSS in drug delivery.[43]

Nanoparticles used for biomedical purposes are often PEGylated. The term PEGylation describes the modification of (mostly) biological molecules by covalent conjugation with polyethylene glycol (PEG), a nontoxic and nonimmunogenic polymer. PEGylation improves drug solubility and stability,[44−46] decreases immunogenicity,[47] and reduces proteolysis.[48,49] In addition, PEGylation controls the transport properties of conjugates, such as the retention time in blood and the renal excretion. Optimization of the nanoparticles' transportation characteristics requires an understanding of their molecular motions and that places a premium on the knowledge of molecular dynamics.

In this study, we attach poly(propylene oxide)/poly(ethylene oxide), PPO/PEO, copolymers to POSS nanoparticles by chemical reaction between the functional end groups on the PPO block (amine) and the POSS side chain (epoxy) in order to synthesize PEGylated POSS. The acronyms PEG and PEO are used interchangeably and here we select to use PEO. The PPO/PEO copolymers are employed for PEGylation for several reasons. First, it is of interest to understand the effect of copolymer composition on the dynamics of copolymers and PEGylated POSS. Hydrophobic/hydrophilic character, morphology and dynamics are all a function of copolymer composition.[50] Second, the presence of a PPO block in the copolymer enables one to analyze the global chain motion by dielectric relaxation spectroscopy (DRS). This is because PPO contains type A dipoles,

*To whom correspondence should be addressed. E-mail: jmijovic@poly.edu.

Published on Web 05/08/2009

parallel to the polymer backbone, which relax via the normal mode process (the α_N process), in addition to type B dipoles that are contributed by the transverse dipole moment component and which relax via the segmental process (the α process).[51−54] The presence of type A dipoles makes it possible to compare dielectric and viscoelastic measurements.

The principal objective of this study is to elucidate the effect of copolymer composition (by varying molecular weight and PPO/PEO mole ratio) on the dynamics of copolymers and PEGylated POSS. To the best of our knowledge, this study marks the first time that POSS is PEGylated by PPO/PEO diblock copolymers and studied by dielectric and dynamic mechanical spectroscopy.

Experimental Section

Materials. *PPO/PEO Copolymers.* Four PPO/PEO copolymers (JEFFAMINE monoamine) were obtained from Huntsman (www.huntsman.com). These copolymers contain two blocks; polypropylene oxide (PPO) end-functionalized with an amine group and polyethylene oxide (PEO) with a methyl end group (Figure 1). The characteristics of copolymers are summarized in Table 1. Copolymers are described by their molecular weight (in Da) followed by the letter "M" that stands for the *monoamine* end group on the PPO block.

Multifunctional POSS. A multifunctional POSS monomer, octaepoxycyclohexyldimethylsilyl−POSS (OC), with a hybrid inorganic−organic three-dimensional structure and eight organic side chains end-functionalized with an epoxy group was obtained from Hybrid Plastic (www.hybridplastics.com). The dimension of the POSS cubic frame, shown in Figure 2, is 1.2−1.5 nm. OC was selected because the cyclohexyl ring in the side chain promotes the formation of linear tether between the epoxy group (on OC) and the primary amine group (on the PPO block), while sterically hindering the secondary amine/epoxy reaction.[55−57]

PEGylated OC. OC and a copolymer were mixed in the stoichiometric ratio (mole ratio 1:8) in toluene using a high-speed stirrer. Toluene provides a good dispersion of OC in the copolymer and is readily removed by evaporation. The primary amine−epoxy reaction was conducted at 353 K. The sample codes for PEGylated OC are listed in Table 2. The first two letters describe the POSS (i.e., OC) and the third one, "M", indicates that the monoamine end-functionalized copolymer has been covalently attached to OC. The number that completes the code is the molecular weight of the copolymer in Da.

Techniques. *Dielectric Relaxation Spectroscopy (DRS).* Our facility combines commercial and custom-made instruments that include (1) a Novocontrol α high-resolution dielectric analyzer (3 μHz to 10 MHz) and (2) a Hewlett-Packard 4291B RF impedance analyzer (1 MHz to 1.8 GHz). Both instruments are interfaced to computers and equipped with heating/cooling controls, including the Novocool system custom-modified for measurements over the frequency range from 3 μHz to 1.8 GHz. In a DRS test, the sample is placed between the stainless steel electrodes. The diameter of the electrodes is 12 mm, and the sample thickness is 0.05 mm. Further details of our DRS facility have been reported previously.[58−60]

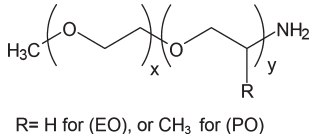

Figure 1. PPO/PEO copolymer architecture.

Fourier Transform Infrared Spectroscopy (FTIR). FTIR spectroscopy was performed using a Nicolet Magna-IR system 750 spectrometer with spectral range from 15800 to 50 cm^{-1} and the Vectra interferometer with resolution better than 0.1 cm^{-1}. Near-infrared (NIR) data were obtained using a calcium fluoride beam splitter, a white light source and a mercury−cadmium−tellurium (MCT) detector. The details of our use of this technique are found elsewhere.[61]

Differential Scanning Calorimetry (DSC). A TA Instrument Co. modulated DSC Q2000 was used. The samples were placed in sealed DSC pans and scanned at a heating or cooling rate of 10 K/min.

Analytical Ultracentrifugation (AUC). Sedimentation velocity tests were carried out on a Beckman Coulter Optima XL-I analytical ultracentrifuge equipped with both absorbance and interference optical detectors. The rotor speed was set at 40000 rpm, and the temperature was maintained at 298 K. The tests were run after the pressure dropped below 5 μmHg. The sedimentation velocity data were analyzed using SEDFIT 92 software to obtain information on the molecular size. All samples were tested at the concentration of 1 g/mL in water. Further details about AUC testing are available elsewhere.[62]

Results and Discussion

This section is organized in three parts as follows. We first recap the dynamics of the individual components, starting with OC. This is followed by a discussion of the dynamics of PPO, PEO and the PPO/PEO copolymers. Finally, we describe the dynamics of PEGylated copolymers obtained by the chemical reaction between the functional end groups on the PPO block (amine) and OC (epoxy).

1. Octaepoxycyclohexyldimethylsilyl−POSS (OC). We recently reported on the molecular dynamics of OC nanoparticles,[57,63] and hence our goal here is not to be comprehensive. Nonetheless, we will briefly summarize the DRS findings that are relevant to this study. Neat OC is a solid at room temperature, insoluble in water and with a melting point at 398 K.

DRS is our principal tool in the study of dynamics. The background on the dielectric properties of glass formers has been well documented in books and key reviews.[61,64−67] The experimentally obtained dielectric spectra in this study were deconvoluted using a sum of the well-known Havriliak−Negami (HN) functional[68] form and the conductivity term:

$$\varepsilon^*(\omega) = \varepsilon' - i\varepsilon'' = \sum_{k=1}^{n}\left[\varepsilon_{\infty k} + \frac{\varepsilon_{0k} - \varepsilon_{\infty k}}{\left(1 + (i\omega\tau_k)^{a_k}\right)^{b_k}}\right] - i\left(\frac{\sigma}{\omega\varepsilon_v}\right)^N \quad (1)$$

where a_k and b_k are the shape parameters that define the breadth and the symmetry of the spectrum, respectively, σ s the conductivity parameter, ε_v is the vacuum permittivity and τ_k is the average relaxation time obtained from the fits. The HN function simplifies to the Debye equation when $a = b = 1$ and the Cole−Cole equation when $b = 1$.[69]

Table 1. PPO/PEO Copolymers Investigated

code	PO/EO mol ratio	MW (Da)	RT appearance	solubility (water %)	degree of crystallinity (%)	T_g (K)	T_m (K)
M600	9/1	600	liquid	0.1−1			
M1000	3/19	1000	waxy solid	100	67		301
M2005	29/6	2000	liquid	<0.1		198	
M2070	10/31	2000	semisolid	100	27	200	282

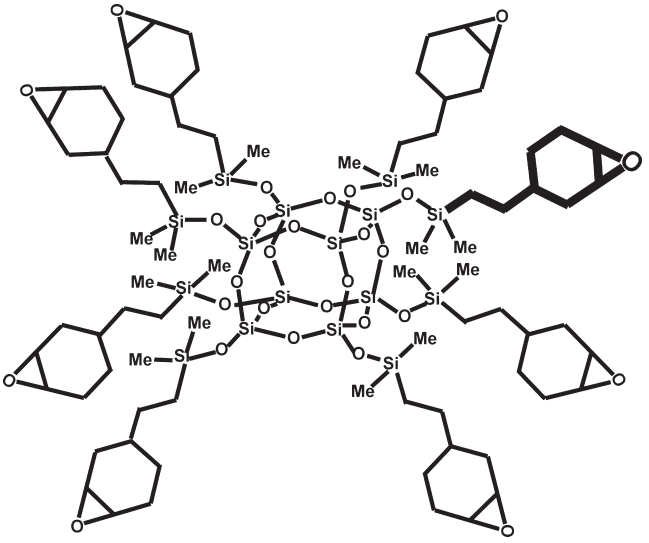

Figure 2. Chemical structure of octaepoxycyclohexyldimethylsilyl−POSS (OC).

Table 2. PEGylated OC Samples Investigated

code	MW (Da)	RT appearance	solubility (water %)	T_g (K)	T_m (K)
OCM600	6800	liquid	< 0.1		
OCM1000	10000	liquid	100		295
OCM2005	18000	liquid	< 0.1	203	
OCM2070	18000	liquid	100	204	270

OC shows two relaxation processes (α_{OC} and β_{OC} in the order of increasing frequency at constant temperature) in the frequency range between 10^{-2} and 10^{6} Hz and in the temperature range between 173 and 373 K. The α_{OC} process is due to the motions of side chains (eight functional chains attached to the silicone and oxygen frame of POSS) and the β_{OC} process originates from the end-group motions (epoxy group on the cyclohexyl). The dielectric relaxation strength decreases for the α_{OC} process and increases for the β_{OC} process with increasing temperature. The temperature dependence of the average relaxation time, τ, for the α_{OC} process follows the Vogel−Fulcher−Tammann (VFT) form:[61,64]

$$\tau = \tau_0 \exp\left(\frac{B}{T - T_v}\right) \quad (2)$$

The Arrhenius form describes the β_{OC} process in OC.

2. PPO, PEO, and PPO/PEO Copolymers. We start with a recap of the morphological and thermal characteristics of PPO, PEO, and PPO/PEO copolymers. PPO can have different end groups, such as hydroxyl or amine, and that will have a small effect on its thermal properties. Neat PPO with hydroxyl end groups is an amorphous polymer and its glass transition temperature (T_g) is 205 K for molecular weight above 400 Da.[70] PEO is a semicystalline polymer, and its melting temperature increases from 324 to 337 K in the molecular weight range from 1.5×10^3 to 3.0×10^5 Da.[71] The T_g of PEO increases with decreasing molecular weight. For example, the T_g values of PEO with molecular weights of 4.0×10^3 Da and 2.0×10^4 Da are 251 and 235 K, respectively.[72] Four PPO/PEO copolymers are studied in this work. M600 and M2005 are amorphous, while M1000 and M2070 are semicrystalline. The DSC glass transition temperatures (T_g) for M2005 and M2070 are 198 and 200 K respectively, while the glass transitions of M600 and M1000 were not observed in the temperature range from 183 to 473 K. The DSC melting points of M1000 and M2070 are 301 and 282 K, respectively. The degree of crystallinity (X_c) of copolymers was calculated based on the enthalpy of melting.[50,73] The X_c values for M1000 and M2070 were found to be 67% and 27%, respectively. A summary of the thermal characteristics of all copolymers is given in Table 1.

The dielectric response of the neat PPO and PEO has been reported[51,53,54,59,60] and a brief recap will suffice here. PPO shows four dielectric relaxations in the order of increasing frequency at constant temperature: the normal mode process ($\alpha_{N\text{-}PPO}$), the segmental process (α_{PPO}) and two local processes, β_{PPO} and γ_{PPO}.[74] An increase in molecular weight slows down the normal mode process but does not affect the segmental process. These two processes overlap for molecular weight below 2 kg/mol. The temperature dependence of the relaxation time for the segmental (τ_S) and the normal mode (τ_N) process is of the Vogel−Fulcher−Tammann (VFT) type. The β_{PPO} process, a secondary relaxation, is present below and above the glass transition temperature (T_g) and it gradually overlaps with the α_{PPO} process with increasing temperature above T_g.[75,76] The γ_{PPO} process reflects the local motions with the shortest time scale.[77,78] The temperature dependence of the average relaxation time for the β_{PPO} and the γ_{PPO} process is Arrhenius-like.

PEO undergoes two dielectric relaxations, termed α_{PEO} and β_{PEO}, in the order of increasing frequency at constant temperature.[78] The α_{PEO} process is due to the segmental motions in the amorphous region of PEO. The temperature dependence of the average relaxation time for the α_{PEO} process is of the VFT form. The β_{PEO} process is due to the local twisting motion in the main chain in the amorphous regions and defective regions within the crystal phase.[65,77,78] This is consistent with the observed local motions in semicrystalline polymers and single crystals.[78] The temperature dependence of the average relaxation time for the β_{PEO} process is of the Arrhenius type. An earlier DMS study has reported the presence of another process, termed $\alpha_{C\text{-}PEO}$, assigned to chain twisting within the crystals.[64] However, this process is masked by high conductivity at low frequencies and cannot be deconvoluted in the dielectric spectrum.

The extent to which the dynamics of neat PPO and PEO are preserved in their block copolymers depends on the molecular weight, the mole ratio of the two blocks and morphology. In Figure 3, we show dielectric loss in the frequency domain with temperature as a parameter for M600 Figure 3A), M1000 (Figure 3B), M2005 Figure 3C) and M2070 Figure 3D). In amorphous copolymers, M600 and M2005, we observe segmental (α) and normal mode (α_N) relaxations. In semicrystalline copolymers, M1000 and M2070, we observe one broad relaxation (the α process). All copolymers have local relaxations (β and γ) at higher frequency. As expected, all processes shift to higher frequency with increasing temperature. However, the dielectric spectra of the copolymers are not a weighted combination of the spectra of neat homopolymers, but are affected by the covalent bond between the PEO and PPO blocks, the interactions between the blocks and the degree of crystallinity.

Best fits of the loss spectra were obtained using the HN functional form for the α process (in amorphous copolymers) and the γ process, and the CC functional form for the α_N, the α (in semicrystalline copolymers) and the β process. In the text that follows, we examine the effect of the copolymer molecular weight and the PPO/PEO ratio (and hence morphology) on three principal dynamics parameters: (1) the average relaxation time; (2) the dielectric relaxation strength; and (3) the shape of the relaxation spectrum.

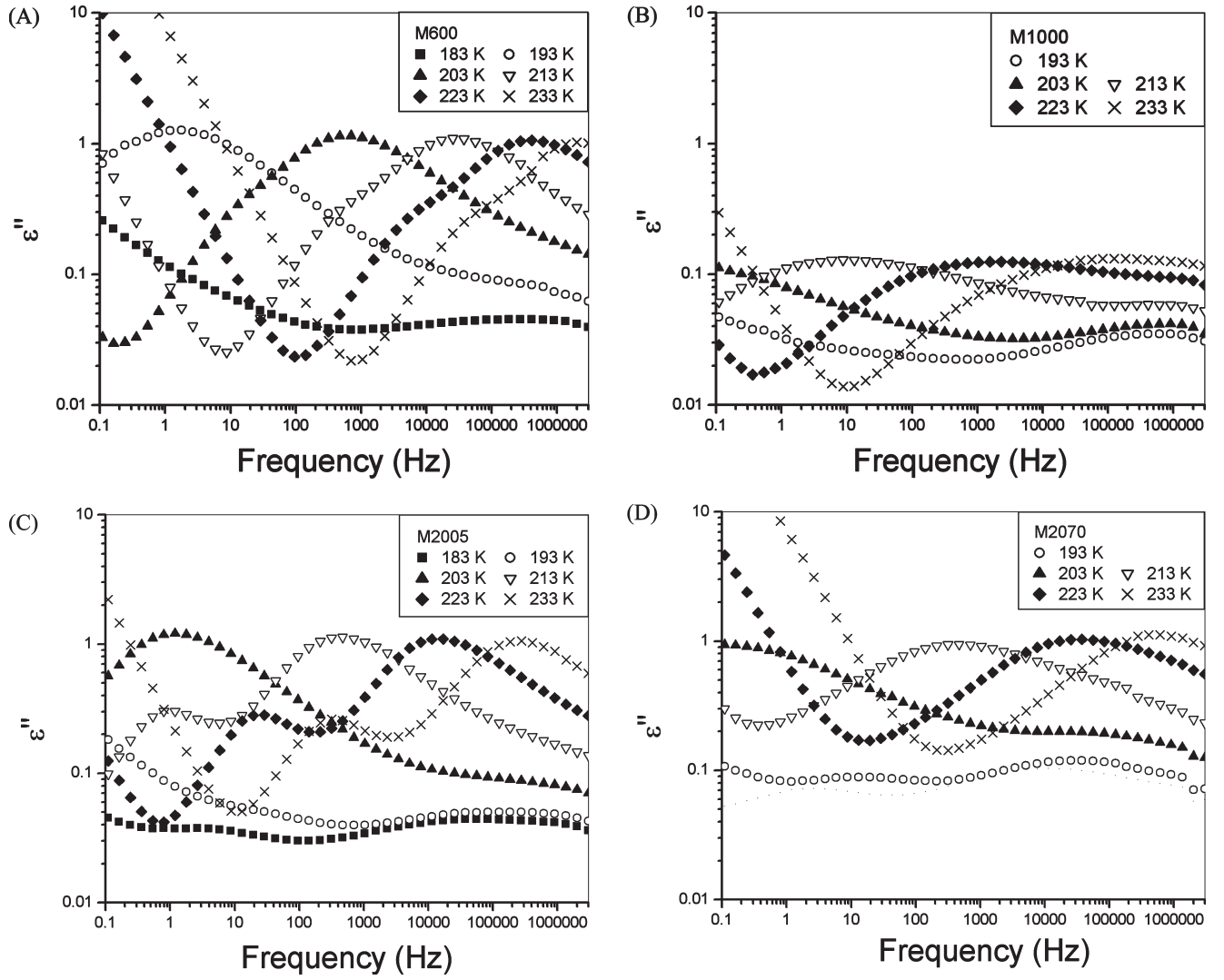

Figure 3. Dielectric loss in the frequency domain with temperature as a parameter for M600 (A), M1000 (B), M2005 (C), and M2070 (D).

Temperature Dependence of the Average Relaxation Time. In the composite plot of Figure 4, parts A and B, we present the temperature dependence of the average relaxation time for various processes in copolymers. The results for the neat PPO and PEO are included for completion.[74,78] M600 and M2005 possess separate segmental and normal mode processes. Previous studies have shown that separate segmental and normal mode relaxations are not discernible in the neat PPO with molecular weight below 2.0×10^3 Da.[59,60] To that end, it is interesting to report that the two amorphous copolymers, M2005 and M600, with the molecular weights of the PPO blocks of 1660 and 540 Da, respectively, show separate segmental and normal mode relaxation. The temperature dependence of the average relaxation time is of the VFT type for both α_N and α relaxation. The normal mode process in the copolymer scales with the PPO molecular weight;[59,60] consequently, the time scale of the average relaxation time (τ_N) is longer in M2005 than in M600. Furthermore, τ_N of M2005 is close to that of the neat PPO2k. This is not surprising because the molecular weight of the PPO block in M2005 of 1660 Da is close to 2000 Da. The time scale of the segmental process in M2005 is one-half decade faster than that of the neat PPO2k, as shown in Figure 4, reflecting the lower glass transition temperature (T_g = 198 K for M2005 and T_g = 205 K for the neat PPO2k). The segmental process in M600 is faster than in the neat PPO400 (T_g = 196 K for the neat PPO400). For example, the relaxation time of the segmental process in M600 at 233 K is about 1 decade shorter than in PPO400.[75] The glass transition temperature of PPO depends on its molecular weight[79,80] and the nature of the end groups.[70,81] Hydrogen bonding through end groups hinders chain motions and contributes to a higher glass transition temperature.[70,81] Neat PPO2k and PPO400 are end-functionalized with hydroxyl groups, while M2005 and M600 have the primary amine group at the end of the PPO block. It is possible that the copolymers have a lower glass transition temperature than the neat PPO due to weaker hydrogen bonding through amine end groups.

Segmental motions in the amorphous regions of semicrystalline polymers above their glass transition temperature are confined by the surrounding lamellar crystals.[82−86] As a consequence of the presence of crystalline regions, the segmental process in the amorphous phase deviates from that in the wholly amorphous polymers. This is usually manifest as follows:[82,87] (1) an increase in the average relaxation time; (2) a decrease in the relaxation strength; (3) an increase in the symmetry and breadth of the relaxation spectrum in comparison with the wholly amorphous sample. Semicrystalline copolymers, M1000 and M2070, show the α process, due to segmental relaxation within the amorphous phase. The temperature dependence of the average relaxation time for

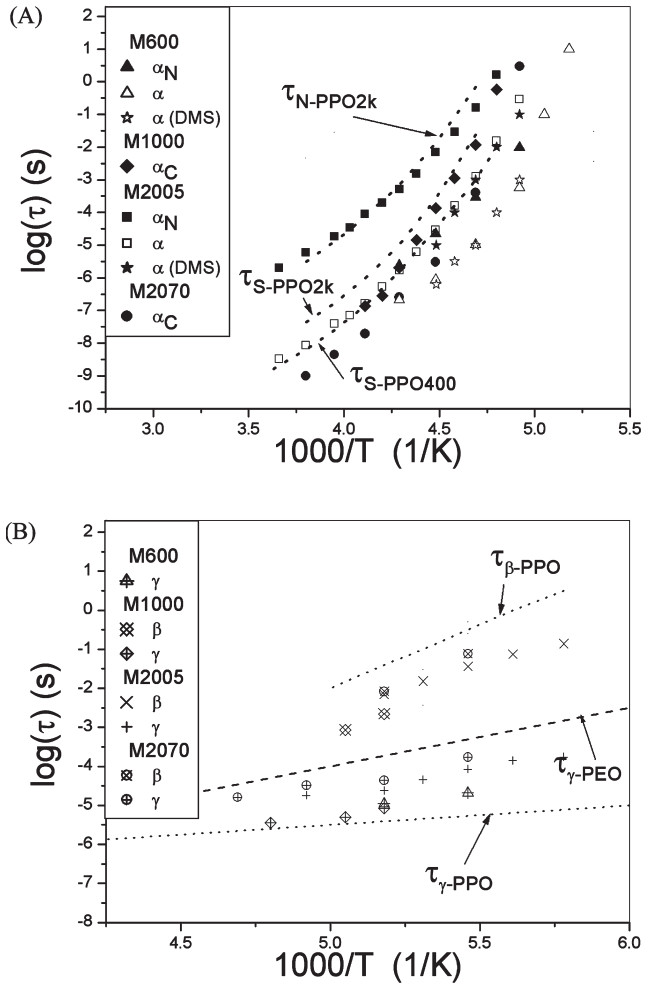

Figure 4. Temperature dependence of the average relaxation time for various relaxation processes A and B in M600, M1000, M2005, and M2070. The data for neat PPO (dotted line) and PEO (dashed line) are included for comparison.

the α process is of the VFT type. The molecular weights of the PPO blocks in M1000 and M2070 are 175 and 625 Da, respectively. The α process is slower in M1000 than M2070 (e.g., 1.5 decade at 213 K), which can be attributed to the higher degree of crystallinity and more pronounced restrictions to the mobility in the amorphous phase caused by the lamellar crystals in the former copolymer. Similar findings have been reported in other semicrystalline polymers.[78,82−89]

All copolymers show the β and the γ processes. The temperature dependence of the average relaxation time for these processes is Arrhenius-like. The β process gradually merges with the segmental process as the temperature is increased above T_g. The β process is attributed to the secondary relaxation of PPO block, since the activation energy of the β process (55 kJ/mol) is close to that of the β_{PPO} process in the neat PPO.[75] The characteristics of the β_{PPO} in PPO are dependent on the hydrogen bonding formed by the end groups.[75,90] The time scale of the β process in copolymers is shorter than in the neat PPO (β_{PPO}) due to the weaker hydrogen bonding through the primary amine end groups on the PPO block. As seen in Figure 4B, the time scale of the γ process in the copolymers falls between the time scale of the γ_{PPO} and the β_{PEO} process. The activation energy of the γ process in the copolymers (25 kJ/mol) is also between that of the γ_{PPO} and the β_{PEO} process (16.8 and 37.8 kJ/mol, respectively).[77,78] Therefore, it can be concluded that the

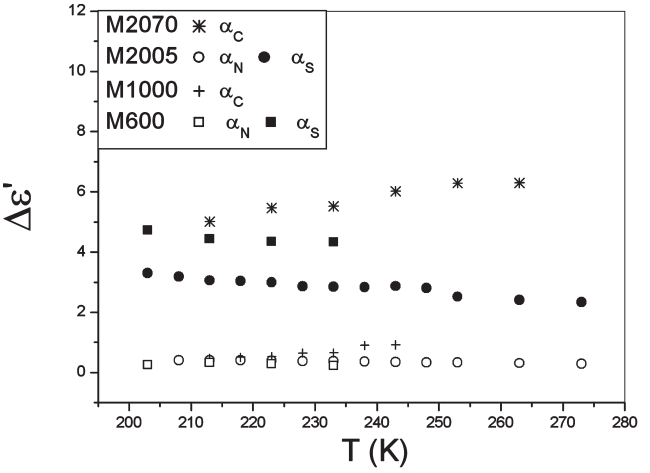

Figure 5. Dielectric relaxation strength as a function of temperature for various relaxations in M600, M1000, M2005, and M2070.

Table 3. Dielectric Strength of Various Relaxation Processes in PPO/PEO Copolymers at 183 and 213 K

materials	α_N(213 K)	α(213 K)	β(183 K)	γ(183 K)
M600	0.33	4.40	not discernible	0.50
M1000	0.70 (α)		0.03	0.43
M2005	0.80	3.80	0.08	0.35
M2070	4.40 (α)		0.36	0.96

γ process in the copolymers is generated by the combination of the γ_{PPO} and the β_{PEO} process.

Relaxation Strength. The relaxation strength ($\Delta\varepsilon$) is an important materials characteristic that is governed by the chemical structure and molecular architecture. It is defined as $\Delta\varepsilon = \varepsilon'_0 - \varepsilon'_\infty$, where ε'_0 and ε'_∞ represent the limiting low- and high-frequency dielectric permittivity and is proportional to the concentration of dipoles and the mean-squared dipole moment per molecule.

The dielectric relaxation strength of the segmental ($\Delta\varepsilon_S$) and the normal mode ($\Delta\varepsilon_N$) process for M600 and M2005 obtained from data fits is shown as a function of temperature in Figure 5. $\Delta\varepsilon_S$ is seen to decrease with increasing temperature for both M600 and M2005, which is in agreement with the previous studies on amorphous polymers.[74] $\Delta\varepsilon_S$ is related to the effective dipole moment (μ_{eff}) in the cooperatively rearranging region (CRR).[30] The size of the CRR increases with decreasing temperature and causes $\Delta\varepsilon_S$ to increase. The dielectric relaxation strength of the normal mode process ($\Delta\varepsilon_N$) is a weak (decreasing) function of temperature, which is also in agreement with the literature,[59,60] though the underlying physics remains incompletely understood. The dielectric relaxation strength of the α process ($\Delta\varepsilon_S$) is greater in M2070 than M1000 due to the lower degree of crystallinity. $\Delta\varepsilon_S$ for M2070 and M1000 increases with increasing temperature, as shown in Figure 5, which is in agreement with the previous studies of segmental motions in the amorphous phase of crystalline polymers.[91,92] The dielectric relaxation strength of the β ($\Delta\varepsilon_\beta$) and the γ ($\Delta\varepsilon_\gamma$) process for all copolymers increases with increasing temperature. The dielectric strength of various relaxation processes in PPO/PEO copolymers at select temperatures is summarized in Table 3.

Relaxation Spectra. Relaxation spectra are described with the HN parameters **a** and **b** that define the spectral breadth and symmetry, respectively. The processes observed in the four copolymers are thermodielectrically simple in the temperature range of our DRS measurements and the parameters **a** and **b** extracted from the data are shown in Table 4.

For the copolymers with the same morphological characteristics (i.e., semicrystalline, M1000 and M2070, or amorphous, M600 and M2005), the difference in **a** is small and in **b** none. Parameter **a** of the α process in semicrystalline copolymers is lower than that of the α process in wholly amorphous polymers.[82−86] Lamellar crystals restrict the available chain conformations in the amorphous phase and that, in turn, causes the spectra to broaden and become symmetric. Parameter **b** is equal to 1 for the α process.

For the β process, parameters **a** and **b** are 0.44 and 1.0 for semicrystalline copolymers and 0.5 and 1.0 for amorphous copolymers, respectively. The β process is symmetric, like the β_{PPO} in the neat PPO.[75] Parameters **a** and **b** for the γ process remain the same in all copolymers, implying that these local motions are not affected by the presence of lamellar crystals.

The results of dynamic mechanical spectroscopy (DMS) are examined next. Figure 6 shows storage (G') and loss (G'') modulus of M2005 in the frequency domain with temperature as a parameter. The results depict the time−temperature superposed master curves constructed using the horizontal shift factors. The average DMS relaxation time for the segmental process was determined from $\tau_S = 1/\omega_{max} = 1/(2\pi f_{max})$ and is shown in Figure 4A. The average relaxation time for the normal mode process was not calculated because of the difficulties in deconvoluting normal mode relaxation from the DMS spectra with sufficient level of confidence. The time scale of the segmental process obtained from DRS is in good agreement with the DMS result, as illustrated in Figure 4A. The same phenomenon was observed in the neat PPO.[59] The DMS results for semicrystalline copolymers are not reported because of high data scatter.

3. PEGylated OC. PEGylated OC, termed OCM, was synthesized by covalently attaching the PPO/PEO copolymers to the OC side chains by the chemical reaction between the functional end groups, primary amine and epoxy. Only linear tethers form between the OC side chains and the copolymer due to the steric hindrance introduced by the cyclohexyl ring that impedes the secondary amine/epoxy reaction.[55−57] The reaction was conducted at 353 K and its progress was monitored with near-infrared (NIR) spectroscopy. The absorption intensities of reactive groups decrease during reaction and vanish in the fully reacted OCM. In the mid-IR spectra, we observe a pronounced peak at ∼1100 cm^{-1} due to the symmetric vibration of Si−O groups in the POSS cage. The presence of this peak[93,94] in all spectra indicates that the POSS cube structure remains unperturbed by the reaction; a degraded cube structure has been shown to result in a broader and asymmetric Si−O peak.[95−97] DSC results also show that copolymers and OC remain stable at 373 K, well above the reaction temperature of 353 K.

Table 4. HN Parameters a and b for Various Relaxation Processes in PPO/PEO Copolymers

materials	α_N(**a**, **b**)	α(**a**, **b**)	β(**a**, **b**)	γ(**a**, **b**)
M600	0.90, 1.0	0.73, 0.50	not discernible	0.46, 0.20
M1000	0.40, 1.0 (α)		0.44, 1.0	0.46, 0.20
M2005	0.94, 1.0	0.75, 0.50	0.50, 1.0	0.46, 0.20
M2070	0.48, 1.0 (α)		0.44, 1.0	0.46, 0.20

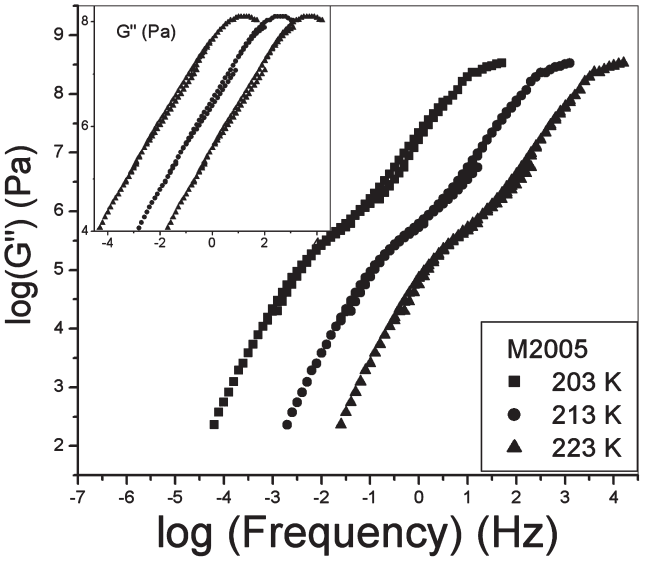

Figure 6. Storage (G') and loss (G'') (inset) modulus of M2005 in the frequency domain with temperature as a parameter.

To identify the molecular weight of OCM, we employed analytical ultracentrifugation (AUC), a powerful technique for monitoring the size, molecular weight and dispersion of particles in water. The solubility of OCM in water is determined by the copolymer composition. In this study, only OCM1000 and OCM2070 are tested, because they are water-soluble. We observe two types of aggregates along with the single dispersed OCM2070 by the mass distribution over molecular weight. The molecular weight of OCM2070 is 18570 Da and hence we estimate that the observed aggregates with molecular weights around 168300 and 216200 Da have the aggregate numbers of 9 and 11, respectively. Similar phenomenon was observed for OCM1000, where the two aggregates have aggregate numbers of 6 and 9. Further study of the mechanism of aggregation of the PEGylated POSS was beyond the scope of this work but is warranted. Upon PEGylation, all four OCM are liquid at room temperature. The thermal properties of OCM are different from those of the neat OC or the corresponding copolymers and are summarized in Table 2. The exact value of the degree of crystallinity (X_c) for OCM1000 and OCM2070 is difficult to determine because of the difficulty in obtaining the enthalpy of melting for the 100% crystalline OC.

Dielectric loss in the frequency domain with temperature as a parameter for OCM600, OCM1000, OCM2005, and OCM2070 is shown in Figure 7. OCM600 shows one broad process at lower frequency, termed α_M, and we see no evidence of separate segmental and normal mode relaxation as in M600. In OCM2005, however, we detect separate segmental and normal mode processes. The α process is also observed in OCM2070. Deconvolution of the α process in OCM1000 is made difficult by the low relaxation strength and hence we omit the analysis of this process. All OCM exhibit local relaxations (β and γ). Dielectric loss spectra were fitted to the HN functional form for the α process in amorphous OCM and the γ process, and to the CC functional form for the α_N, the α (in semicrystalline OCM), the α_M and the β process. In the text below, we contrast the dynamics of each OCM with the corresponding neat copolymer in terms of the following parameters: the average relaxation time, the dielectric relaxation strength and the shape of the relaxation spectrum.. *Temperature Dependence of the Average Relaxation Time*. We consider amorphous OCM first. The temperature dependence of the average relaxation time for various processes in OCM600 and OCM2005 is illustrated in Figure 8. The data for the corresponding neat copolymers (M600 and M2005) are included for comparison. From Figure 8 we make two observations: (1) the α_M process in OCM600 has a longer time scale than the normal mode process in M600, and (2) segmental and normal mode relaxations in OCM2005

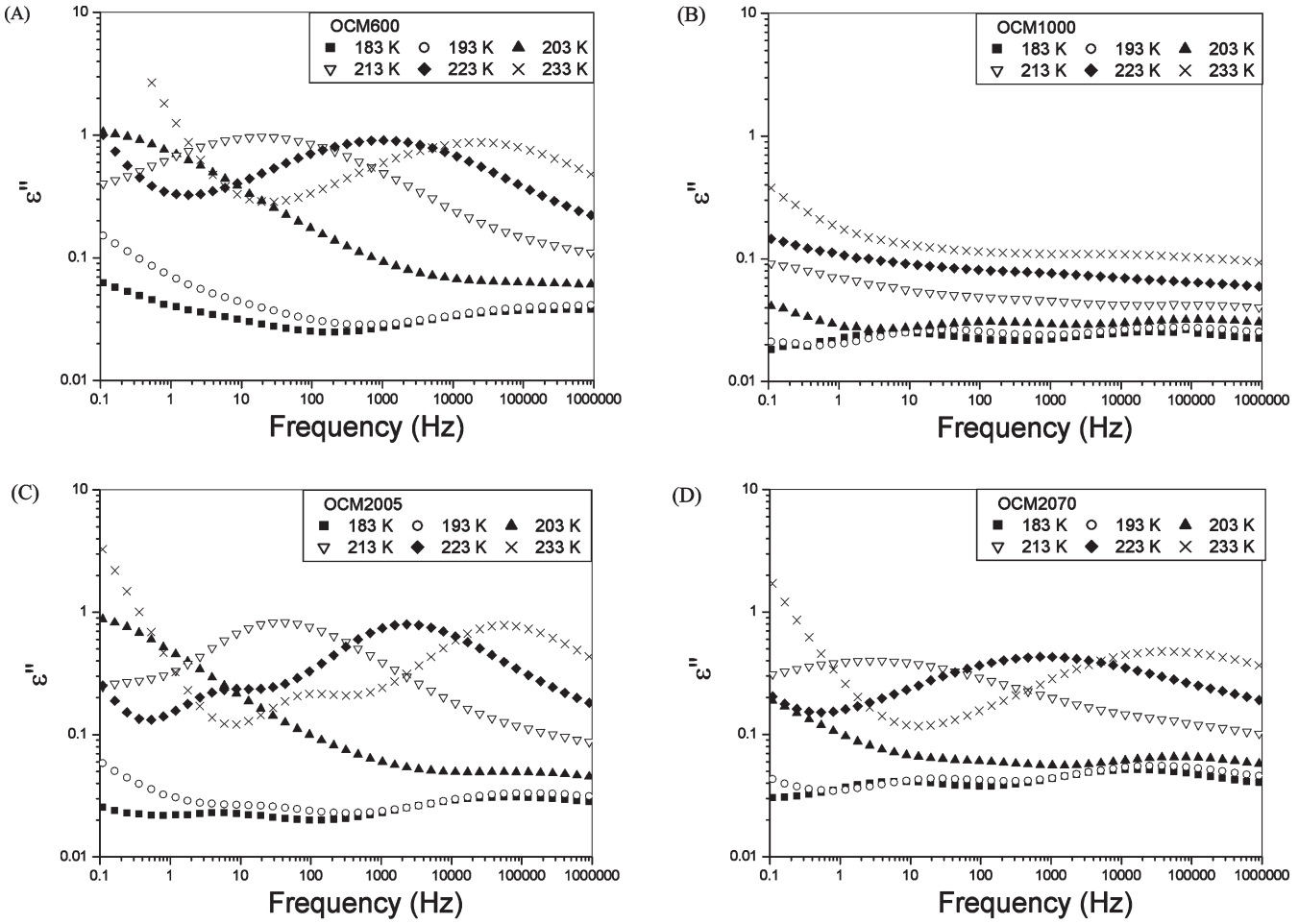

Figure 7. Dielectric loss in the frequency domain with temperature as a parameter for OCM600 (A), OCM1000 (B), OCM2005 (C), and OCM2070 (D).

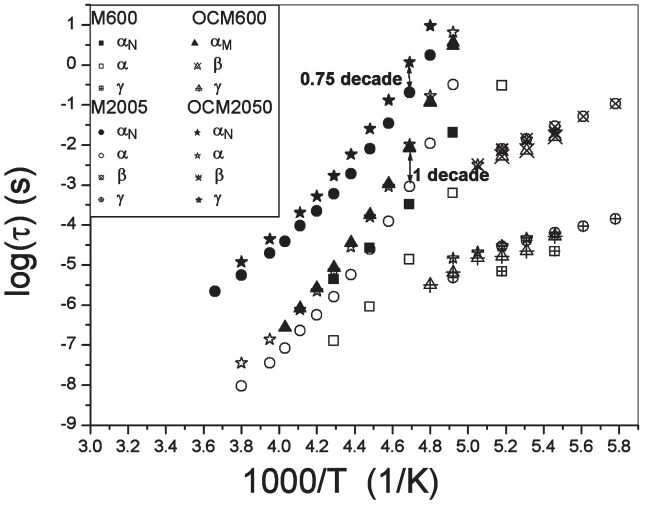

Figure 8. Temperature dependence of the average relaxation time for various relaxation processes in OCM600 and OCM2005. Results for M600 and M2005 are included for comparison.

have a longer time scale than the corresponding processes in M2005. The α_M process in OCM600 and OCM2005 originates in the motions of copolymer chains extended by the covalently bonded OC side chains. The difference in the dynamics of the neat copolymer and the PEGylated OC is thus traced to the formation of a new chain formed by covalent bonding of OC to the copolymer. The local process in the neat OC originates from the end functional group (epoxy) in the side chains[63] and vanishes after PEGylation. The average relaxation time of the β and the γ process in OCM600 and OCM2005 does not differ appreciably from the values for the corresponding copolymer, suggesting that the time scales of those motions are not affected by the covalent bonding between OC and the copolymer.

The temperature dependence of the average relaxation time for the semicrystalline copolymers, OCM1000 and OCM2070, is illustrated in Figure 9. Data for the corresponding copolymers are also included for comparison. The time scale of the α process in OCM2070 is longer than in M2070. For example, the α process in OCM2070 at 213K is shifted to lower frequency by 2 decades in comparison with the same process in M2070. The average relaxation time of the β and the γ process in OCM1000 and OCM2070 lies in the same frequency range as in the corresponding copolymer. We conclude that the PEGylated OC exhibits longer time scale of segmental and normal mode relaxation in comparison with the corresponding neat copolymer, while the time scale of the β and the γ process remains unaffected by PEGylation.

Dielectric Relaxation Strength. We first consider the temperature dependence of the dielectric strength ($\Delta\varepsilon$). In OCM600, $\Delta\varepsilon$ of the α_M process decreases with increasing temperature. In OCM2005 and OCM2070 all relaxation processes follow the same temperature dependence as in the neat copolymers.

It is also of interest is to compare $\Delta\varepsilon$in OCM and the neat copolymer at a constant temperature. All relaxations (α, α_N,

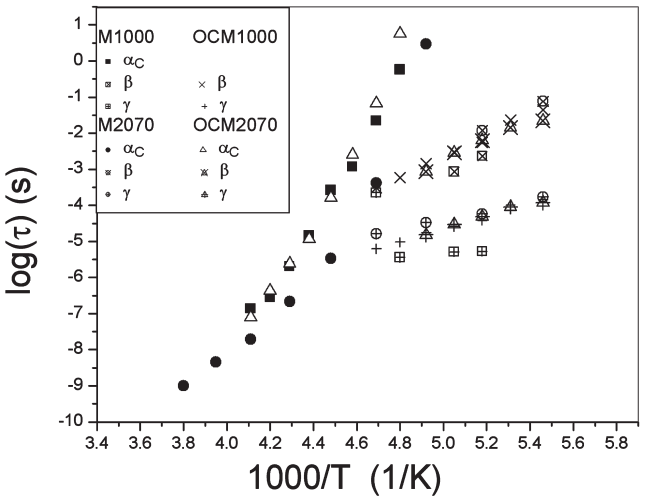

Figure 9. Temperature dependence of the average relaxation time for various relaxation processes in OCM1000 and OCM2070. Results for M1000 and M2070 are included for comparison.

Table 5. Dielectric Strength of Various Relaxation Processes in OCM at 183 and 213 K

materials	α_N(213 K)	α(213 K)	β(183 K)	γ(183 K)
OCM600	4.30 (α_M)		0.02	0.40
OCM1000			0.02	0.29
OCM2005	0.69	3.50	0.07	0.32
OCM2070	3.06 (α)		0.15	0.47

Table 6. HN Parameters a and b for Various Relaxation Processes in OCM

materials	α_N (**a**, **b**)	α (**a**, **b**)	β(**a**, **b**)	γ(**a**, **b**)
OCM600	0.40, 1.0 (α_M)		0.50, 1.0	0.46, 0.20
OCM1000	-		0.44, 1.0	0.46, 0.20
OCM2005	0.68, 1.0	0.72, 0.50	0.50, 1.0	0.46, 0.20
OCM2070	0.32, 1.0 (α)		0.44, 1.0	0.46, 0.20

β and γ) in OCM2005 and OCM2070 exhibit lower $\Delta\varepsilon$ than the corresponding copolymer; however, further investigation is needed to clarify the underlying mechanism for each process Examples of $\Delta\varepsilon$ values for segmental and chain motions at 213 K and local motions at 183 K are illustrated in Table 5.

Relaxation Spectra. All processes in OCM are thermodielectrically simple and their HN parameters **a** and **b** are listed in Table 6. The α_M process in OCM600 is symmetric and broader than either the segmental or the normal mode process in M600. Parameter **a** of the segmental and the normal mode process in OCM2005 is lower than in M2005, while parameter **b** is constant. The same trend for the α process was observed in OCM2070. The observed spectral broadening in OCM implies a wider distribution in the time scale of relaxation and suggests that the covalent bonding between OC and the copolymer restricts chain mobility. Parameters **a** and **b** for the β and the γ process in OCM do not differ from those in the neat copolymers.

The results of dynamic mechanical spectroscopy (DMS) are described next. Storage and loss (inset) modulus in the frequency domain for M600, M2005, OCM600, and OCM2005 at 203 K are shown in Figure 10. Data were shifted with respect to the reference curve at 203 K. An increase in the time scale of the segmental and the normal mode process in OCM in comparison with the corresponding neat copolymer is observed and that finding parallels the DRS results. The observed increase in G' and G'' of OCM is due to the incorporation of the rigid OC nanoparticles. In the

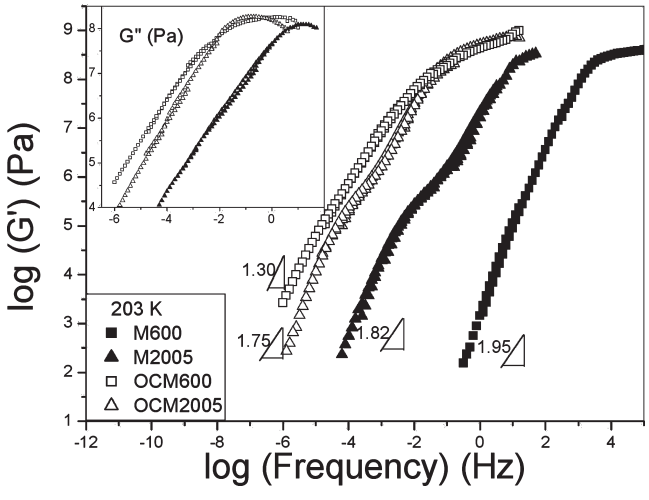

Figure 10. Storage (G') and loss (G'') (inset) modulus in the frequency domain for M600, M2005, OCM600 and OCM2005 at 203 K. The curves were shifted horizontally using data at 203 K as a reference.

terminal relaxation zone of M600 and M2005, the slope of G' vs ω is 1.95 and 1.82, respectively. Upon PEGylation, the slope decreases to 1.30 and 1.75, respectively. The decrease in the slope signifies higher viscosity in OCM due to the covalent bonding between the copolymer and OC. The η_0 was extracted directly from the data by averaging the low shear rate values of η. Identical results were obtained by calculating the zero-shear viscosity from $\eta_0 = \lim\{G''(\omega)/\omega\}$ as $\omega \rightarrow 0$. For example, the value of η_0 at 273 K for M600, M2005, OCM2005 and OCM600 is 0.1 Pa·s, 1.0 Pa·s, 3.8 Pa·s and 5.7 Pa·s, respectively. OCM600 has the highest viscosity due to the highest weight percentage of OC. A direct comparison of DRS and DMS results reveals an excellent agreement between the time scales of the segmental process obtained by those two techniques.

Conclusions

We have completed an investigation of the dynamics of four PPO/PEO copolymers and PEGylated POSS using dielectric relaxation spectroscopy and dynamic mechanical spectroscopy. The effects of the copolymer molecular composition and morphology, PEGylation and temperature on the dynamics of those systems were evaluated and our principal conclusions are summarized below.

The segmental (α), the normal mode (α_N), and two local processes (β and γ) were observed in two amorphous copolymers (M600 and M2005). This is interesting because previous studies have shown that separate segmental and normal mode relaxations are not discernible in the neat PPO with molecular weight below 2000 Da. The time scale of the normal mode process in M600 is shorter than in M2005 due to the lower molecular weight of the PPO block. The segmental process corresponds to the "dielectric" glass transition temperature of the copolymer and depends on the mole ratio of blocks and the nature of end groups. With increasing temperature, the dielectric relaxation strength decreases for the segmental process but increases for the normal mode process. Semicrystalline copolymers, M1000 and M2070, exhibit the α process and two local processes (β and γ). The presence of the α process is due to the segmental relaxation within the amorphous phase between lamellar crystals. Higher degree of crystallinity results in a lower dielectric strength, as evidenced by comparing M1000 with M2070. For all copolymers, the β process is attributed to the secondary relaxation of PPO block and the γ process is generated by the combination of the γ_{PPO} and the β_{PEO} process.

PEGylated POSS, termed OCM, was synthesized by covalently attaching PPO/PEO copolymer to the side chains of OC. The molecular weight of OCM was identified by analytical ultracentrifugation (AUC). A single broad process (α_M) was observed for OCM600. However, OCM2005 exhibits separate segmental and normal mode relaxations with a longer time scale than in the neat M2005. The α process in OCM2070 is also slower than in M2070 and we conclude that the covalent bonding between OC and copolymer slows down the segmental and the normal mode process in this new chain. All PEGylated OCs exhibit the same time scale of the local motions (the β and γ process).

The dynamics of amorphous copolymers and PEGylated POSS were also studied by dynamic mechanical spectroscopy (DMS). The observed increase in G' and G'' of OCM compared with the corresponding neat copolymer is due to the incorporation of rigid POSS nanoparticles. The decreasing slope of G' vs ω in the terminal relaxation zone is the result of increased viscosity after PEGylation. OCM600 shows highest viscosity due to the highest weight percentage of POSS. A comparative analysis of DRS and DMS data shows that the time scale of the segmental process obtained from DRS and DMS is in excellent agreement.

Acknowledgment. This work is supported by the National Science Foundation under Grant DMR-0346435.

References and Notes

(1) Zeis, R.; Mathur, A.; Fritz, G.; Lee, J.; Erlebacher, J. *J. Power Sources* **2007**, *165*, 65.
(2) Liu, S.; Jaffrezic, N.; Guillard, C. *Appl. Surf. Sci.* **2008**, *255*, 2704.
(3) Siddiquey, I. A.; Furusawa, T.; Hoshi, Y.; Ukaji, E.; Kurayama, F.; Sato, M.; Suzuki, N. *Appl. Surf. Sci.* **2008**, *255* (5), 2419.
(4) Matykina, E.; Arrabal, R.; Monfort, F.; Skeldon, P.; Thompson, G. E. *Appl. Surf. Sci.* **2008**, *255* (5), 2830.
(5) Hernandez Battez, A.; Gonzalez, R.; Viesca, J. L.; Fernandez, J. E.; Diaz Fernandez, J. M.; Machado, A.; Chou, R.; Riba, J. *Wear* **2008**, *265*, 422.
(6) Langer, R.; Tirrell, D. A. *Nature* **2004**, *428*, 487.
(7) Roco, M. C. *Curr. Opin. Biotechnol.* **2003**, *14* (3), 337.
(8) Prasad, G. L. Biomedical Applications of Nanoparticles. In *Nanostructure Science and Technology*; Lockwood, D. J., Ed.; Spring New York: New York, **2008**.
(9) Pantarotto, D.; Partidos, C. D.; Hoebeke, J.; Brown, F.; Kramer, E.; Briand, J. P.; Muller, S.; Prato, M.; Bianco, A. *Chem. Biol.* **2003**, *10*, 961–966.
(10) Nam, J. M.; Thaxton, C. S.; Mirkin, C. A. *Science* **2003**, *301* (5641), 1884.
(11) Mahtab, R.; Rogers, J. P.; Murphy, C. J. *J. Am. Chem. Soc.* **1995**, *117*, 9099.
(12) Ma, J.; Wong, H.; Kong, L. B.; Peng, K. W. *Nanotechnology* **2003**, *14*, 619.
(13) Chen, H.; Zheng, Y.; Jiang, J.-H.; Wu, H.-L.; Shen, G.-L.; Yu, R.-Q. *Biosens. Bioelectron.* **2008**, *24*, 684.
(14) Gowen, B. B.; Fairman, J.; Dow, S.; Troyer, R.; Wong, M. H.; Jung, K. H.; Melby, P. C.; Morrey, J. D. *Antiviral Res.* **2009**, *81* (1), 37.
(15) Środa, K.; Michalak, K.; Maniewska, J.; Grynkiewicz, G.; Szeja, W.; Zawisza, J.; Hendrich, A. B. *Biophys. Chem.* **2008**, *138* (3), 78.
(16) Jones, M.-C.; Gao, H.; Leroux, J.-C. *J. Controlled Release* **2008**, *132* (3), 208.
(17) Liu, Y.; Cao, X.; Luo, M.; Le, Z.; Xu, W. *J. Colloid Interface Sci.* **2008**, *329* (2), 244.
(18) Lecommandoux, S.; Sandre, O.; Checot, F.; Perzynski, R. *Prog. Solid State Chem.* **2006**, *34*, 171.
(19) McCarthy, J. R.; Perez, J. M.; Bruckner, C.; Weissleder, R. *Nano Lett.* **2005**, *5* (12), 2552.
(20) Liu, Y.; Wu, D. C.; Zhang, W. D.; Jiang, X.; He, C. B.; Chung, T. S.; Coh, S. H.; Leong, K. W. *Angew. Chem., Int. Ed.* **2005**, *44*, 4782.
(21) Yang, N.; Uetsuka, H.; Osawa, E.; Nebel, C. E. *Angew. Chem., Int. Ed.* **2008**, *47*, 5183.
(22) Feazell, R. P.; Nakayama-Ratchford, N.; Dai, H.; Lippard, S. J. *J. Am. Chem. Soc.* **2007**, *129*, 8438.
(23) Chen, X.; Kis, A.; Zettl, A.; Bertozzi, C. R. *Proc. Natl. Acad. Sci. U. S.A.* **2007**, *104*, 8218.
(24) Singh, R.; Pantarotto, D.; Lacerda, L.; Pastorin, G.; Klumpp, C.; Prato, M.; Bianco, A.; Kostarelos, K. *Proc. Natl. Acad. Sci.* **2006**, *103*, 3357.
(25) Jin, H.; Heller, D. A.; Strano, M. S. *Nano Lett.* **2008**, *8*, 1577.
(26) Rajan, A.; Strano, M. S.; Heller, D. A.; Hertel, T.; Schulten, K. *J. Phys. Chem. B* **2008**, *112*, 6211.
(27) Strano, M. S.; Jin, H. *ACS Nano* **2008**, *2*, 1749.
(28) Fantini, C.; Pimenta, M. A.; Strano, M. S. *J. Phys. Chem. C* **2008**, *112*, 13150.
(29) Lee, C. Y.; Sharma, R.; Radadia, A. D.; Masel, R. I.; Strano, M. S. *Angew. Chem., Int. Ed.* **2008**, *47*, 5018.
(30) Gao, X.; Cui, Y.; Levenson, R. M.; Chung, L. W. K.; Nie, S. *Nat. Biotechnol.* **2004**, *22* (8), 969.
(31) Lin, Y.; Boker, A.; He, J.; Sill, K.; Xiang, H.; Abetz, C.; Li, X.; Wang, J.; Emrick, T.; Long, S.; Wang, Q.; Balazs, A.; Russell, T. P. *Nature* **2005**, *434*, 55.
(32) Sounderya, N.; Zhang, Y. *Rec. Patents Biomed. Eng.* **2008**, *1*, 34.
(33) Pielichowski, K.; Njuguna, J.; Janowski, B.; Pielichowski, J. *Adv. Polym. Sci.* **2006**, *201*, 225.
(34) Lucke, S.; Stoppek-Langner, K. *Appl. Surf. Sci.* **1999**, *145*, 713.
(35) Schwab, J. J.; Lichtenhan, J. D. *Appl. Organomet. Chem.* **1998**, *12*, 707.
(36) Li, G. Z.; Wang, L. C.; Ni, H. L.; Pittman, C. U. *J. Inorg. Organomet. Polym.* **2001**, *11*, 123.
(37) Carroll, J. B.; Waddon, A. J.; Nakade, H.; Rotello, V. M. *Macromolecules* **2003**, *36*, 6298.
(38) Zheng, L.; Farris, R. J.; Coughlin, E. B. *Macromolecules* **2001**, *34*, 8034.
(39) Zheng, L.; Kasi, R. M.; Farris, R. J.; Coughlin, E. B. *J. Polym. Sci., Part A: Polym. Chem.* **2002**, *40*, 885.
(40) Xu, H. Y.; Kuo, S. W.; Lee, J. S.; Chang, F. C. *Macromolecules* **2002**, *35*, 8788.
(41) Torricelli, P.; Verne, E.; Brovarone, C. V.; Appendino, P.; Rustichelli, F.; Krajewski, A.; Ravaglioli, A.; Pierini, G.; Fini, M.; Giavaresi, G.; Giardino, R. *Biomaterials* **2001**, *22*, 2535.
(42) Wirtz, D.; Fischer, H.; Neuss, M.; Ammenwerth, J.; Niethard, F. U.; Marx, R. *Biomed. Tech.* **2003**, *48*, 154.
(43) McCusker, C.; Carroll, J. B.; Rotello, V. M. *Chem. Commun.* **2005**, (996).
(44) Hedden, R. C.; Bauer, B. J. *Macromolecules* **2003**, *36*, 1829.
(45) D'Emanuele, A.; Attwood, D. *Adv. Drug Deliv. Rev.* **2005**, *57*, 2147.
(46) Svenson, S.; Tomalia, D. A. *Adv. Drug Deliv. Rev.* **2005**, *57*, 2106.
(47) Harris, J. M.; Chess, R. B. *Nat. Rev. Drug Disc.* **2003**, *2*, 214.
(48) Maruyama, K. *Biosci. Rep.* **2002**, *22*, 251.
(49) Allen, C.; Santos, N. D.; Gallagher, R.; Chiu, G. N. C.; Shu, Y.; Li, W. M.; Johnstone, S. A.; Janoff, A. S.; Mayer, L. D.; Webb, M. S.; Bally, M. B. *Biosci. Rep.* **2002**, *22*, 225.
(50) Moreno, S.; Rubio, R. G.; Luengo, G.; Ortega, F.; Prolongo, M. G. *Eur. Phys. J. E* **2001**, *4*, 173.
(51) Stockmayer, W. H.; Baur, M. E. *J. Am. Chem. Soc.* **1964**, *86*, 3485.
(52) Adachi, K.; Kotaka, T. *Prog. Polym. Sci.* **1993**, *18*, 585.
(53) Watanabe, H. *Prog. Polym. Sci.* **1999**, *24*, 1253.
(54) Watanabe, H. *Macromol. Rapid Commun.* **2001**, *22*, 127.
(55) Choi, J.; Yee, A. F.; Laine, R. M. *Macromolecules* **2004**, *37*, 3267.
(56) Choi, J.; Yee, A. F.; Laine, R. M. *Macromolecules* **2003**, *36*, 5666.
(57) Bian, Y.; Mijovic, J. *Macromolecules* **2008**, *41*, 7122.
(58) Mijovic, J.; Miura, N.; Monetta, T.; Duan, Y. *Polym. News* **2001**, *26*, 251.
(59) Mijovic, J.; Sun, M.; Han, Y. *Macromolecules* **2002**, *35*, 6417.
(60) Mijovic, J.; Han, Y.; Sun, M.; Pejanovic, S. *Macromolecules* **2003**, *36*, 4589.
(61) Williams, G. Dielectric relaxation spectroscopy of amorphous polymer systems: the modern approches. In *Keynote Lectures in Selected Topics of Polymer Science*; CSIC: Madrid, **1997**; Vol. Chapter 1, p 1−40.
(62) Lu, S.; Bian, Y.; Zhang, L.; Somasundaran, P. *J. Colloid Interface Sci.* **2007**, *316*, 310.
(63) Bian, Y.; Pejanovic, S.; Kenny, J.; Mijovic, J. *Macromolecules* **2007**, *40*, 6239.
(64) Kremer, F.; Schonhals, A. *Broadband Dielectric Spectroscopy*; Springer-Verlag: Berlin, **2002**.
(65) Runt, J. P.; Fitzgerald, J. J. *Dielectric Spectroscopy of Polymeric Materials Fundamentals and Applications*; American Chemical Society: Washington, DC, **1997**.
(66) Wong, J.; Austin, A. C. *Glass Structure by Spectroscopy*; Marcel Dekker Inc.: New York, **1976**.
(67) Riande, E.; Diaz-Calleja, R. *Electrical Properties of Polymers*; CRC Press: Boca Raton, FL, **2004**.

(68) Havriliak, S.Jr.; Negami, S. *Polymer* **1967**, *8*, 161.
(69) Cole, R. H.; Cole, K. S. *J. Chem. Phys.* **1942**, *10*, 98.
(70) Nicol, E.; Nicolai, T.; Durand, D. *Macromolecules* **1999**, *32*, 7530.
(71) Sengwa, R. J.; Kaur, K.; Chaudhary, R. *Polym. Int.* **2000**, *49*, 599.
(72) Porter, R. S.; Wang, L. H. *J. Therm. Anal.* **1996**, *46*, 871.
(73) O'Malley, J. J.; Crystal, R. G.; Erhardt, P. F. *Block Copolymers*; Aggarwal, S. L., Ed.; Plenum Press: New York, **1970**.
(74) Hedvig, P. *Dielectric Spectroscopy of Polymers*; Halsted Press: New York, **1977**.
(75) Grzybowska, K.; Grzybowski, A.; Ziolo, J.; Paluch, M.; Capaccioli, S. *J. Chem. Phys.* **2006**, *125*, 044904.
(76) Ngai, K. L.; Paluch, M. *J. Chem. Phys.* **2004**, *120*, 857.
(77) Saba, R. G.; Sauer, J. A.; Woodward, A. E. *J. Polym. Sci., Part A: Polym. Chem.* **1963**, *1*, 1483.
(78) McCrum, N. G.; Read, B. E.; Williams, G., *Anelastic and Dielectric Effects in Polymeric Solids*; Dover Publication, Inc.: New York, **1991**.
(79) Nicolai, T.; Floudas, G. *Macromolecules* **1998**, *31*, 2578.
(80) Sperling, L. H. *Introduction to Physical Polymer Science*; Wiley and Sons: New York, **1996**.
(81) Nicol, E.; Durand, D.; Nicolai, T. *Europhys. Lett.* **2001**, *53*, 598.
(82) Coburn, J. C.; Boyd, R. H. *Macromolecules* **1986**, *19*, 2238.
(83) Ezquerra, T. A.; Majszczyk, J.; Balta-Calleja, F. J.; Lopez-Cabarcos, E.; Gardner, K. H.; Hsiao, B. S. *Phys. Rev. B* **1994**, *50*, 6023.
(84) Havens, J. R.; VanderHart, D. L. *Macromolecules* **1985**, *18*, 1663.
(85) Nogales, A.; Denchev, Z.; Ezquerra, T. A. *Macromolecules* **2000**, *33*, 9367.
(86) Williams, G. *Adv. Polym. Sci.* **1979**, *33*, 59.
(87) Nogales, A.; Ezquerra, T. A.; Garcia, J. M.; Balta-calleja, F. J. *J. Polym. Sci., Part B: Polym. Phys.* **1999**, *37*, 37.
(88) Schlosser, E.; Schonhals, A. *Colloid Polym. Sci.* **1989**, *267*, 963.
(89) Lund, R.; Alegría, A.; Goitandía, L.; Colmenero, J.; González, M. A.; Lindner, P. *Macromolecules* **2008**, *41*, 1364.
(90) Pawlus, S.; Hensel-Bielowka, S.; Paluch, M.; Casalini, R.; Roland, C. M. *Phys. Rev. B* **2005**, *72*, 064201.
(91) Mijovic, J.; Sy, J. W.; Kwei, T. K. *Macromolecules* **1997**, *30*, 3042–50.
(92) Sy, J. W.; Mijovic, J. *Macromolecules* **2000**, *33*, 933–46.
(93) Marcolli, C.; Calzaferri, G. *Appl. Organomet. Chem.* **1999**, *13*, 213.
(94) Wallace, W. E.; Guttman, C. M.; Antonucci, J. M. *Polymer* **2000**, *41*, 2219.
(95) Silverstein, R. M.; Webster, F. X.; Kiemle, D. *Spectrometric Identification of Organic Compounds*; John Wiley & Sons: New York, **1996**; p 71.
(96) Chen, Y.; Iroh, J. O. *Chem. Mater.* **1999**, *11*, 1222.
(97) Deng, B.; Hu, Y.; Chen, L.; Chiu, W.; Wu, T. *J. Appl. Polym. Sci.* **1999**, *74*, 229.